buildings

MDPI

Article

Investigation of Key Parameters Influencing Shear Behavior in Glass-Fiber-Reinforced Polymer (GFRP)-Reinforced Concrete (RC) Interior Slab–Column Connections

Loai Alkhattabi [1], Nehal M. Ayash [2], Mohamed Hassan [2,3] and Ahmed Gouda [2,*]

[1] Department of Civil and Environmental Engineering, College of Engineering, University of Jeddah, Jeddah 23890, Saudi Arabia; laalkhattabi@uj.edu.sa
[2] Department of Civil Engineering, Faculty of Engineering, Helwan University (HU), Cairo 11795, Egypt; nehal82ayash@m-eng.helwan.edu.eg (N.M.A.); mohamed.hassan@usherbrooke.ca (M.H.)
[3] Department of Civil Engineering, Université de Sherbrooke, Sherbrooke, QC J1K 2R1, Canada
* Correspondence: ahmed.atef@m-eng.helwan.edu.eg

Abstract: This article explores the punching shear behavior of GFRP-RC interior slab–column connections. The parameters tested included the column–aspect ratio (1.0, 2.0, 3.0, 4.0, and 5.0), perimeter-to-depth ratio for square column stubs with side lengths of 0.3, 0.4, 0.5, 0.6, and 0.7 m, and span-to-depth ratios of 4, 6, 8, 10, and 12. A review of the literature revealed that no previous study has investigated the effect of these parameters or their interactions on this type of connection. Numerically, twenty-five slabs were created using finite element (FE) software (V3), each with square dimensions of 2.5 m and a constant thickness of 0.2 m. The central column extended 0.3 m from the top and bottom of the slab. All four sides of the slabs were supported, and the specimens underwent pure static shear load testing. The test results demonstrated that all slabs failed due to punching shear. Increasing any parameter value reduced the punching shear stresses. Additionally, the results indicated that Canadian (CSA-S806-12) and Japanese (JSCE-97) standards for FRP-RC materials generally provided the closest predictions of punching shear capacity compared to the American guideline, ACI 440.1R-22. However, all standards exhibited shortcomings and require enhancement and modifications, particularly to consider the impact of the span-to-depth ratio. Therefore, three equations were developed to predict the shear strength of the connections, yielding better results than those prescribed by the North American and Japanese standards.

Keywords: punching shear; interior; GFRP; slab–column connection; span-to-depth ratio; perimeter-to-depth ratio; column–aspect ratio

Citation: Alkhattabi, L.; Ayash, N.M.; Hassan, M.; Gouda, A. Investigation of Key Parameters Influencing Shear Behavior in Glass-Fiber-Reinforced Polymer (GFRP)-Reinforced Concrete (RC) Interior Slab–Column Connections. *Buildings* **2024**, *14*, 1251. https://doi.org/10.3390/buildings14051251

Academic Editor: Dongming Li

Received: 27 March 2024
Revised: 13 April 2024
Accepted: 26 April 2024
Published: 28 April 2024

1. Introduction

Faster deterioration and high maintenance costs are associated with parking garages reinforced with steel bars due to the corroded nature of these steel reinforcements. Compared to other building types, especially during the winter months, parking garages experience harsh and unusual weather conditions, particularly in northern and coastal regions, owing to their open design concept. The accumulation of melted snow and deicing salts from vehicles on parking garage surfaces accelerates the corrosion process, compromising the structural integrity of slabs, beams, columns, and even walls. To address this issue, non-corrodible fiber-reinforced polymers (FRP) have been suggested as suitable alternatives to replace steel reinforcements [1,2].

The above-mentioned solution has been utilized to some degree. The Laurier-Tache and La Chanceliere Parking Garages in Quebec, Canada, were rehabilitated using FRP bars. Nevertheless, many questions and concerns have been raised regarding the unknown behavior and interactions between FRP reinforcements and concrete, such as the punching shear strength of FRP reinforced-concrete (RC) interior slab–column connections. These

concerns have spurred civil engineering researchers to explore and understand the behavior of FRP-RC members. Consequently, two projects were designed to address some of these questions. The first project, conducted at the University of Sherbrooke [3,4], examined parameters including the flexural reinforcement ratio, glass and carbon FRP stirrups, slab thickness, and concrete compressive strength. Full-scale slabs were tested under pure shear force, confirming the significant impact of these parameters on the behavior of FRP-RC interior slab–column connections.

The second project, undertaken at the University of Manitoba [5,6], involved testing slabs under a 15% moment-to-shear ratio. The parameters tested included the flexural reinforcement ratio, concrete compressive strength, 15% to 30% moment-to-shear ratio, and shear stud reinforcement. The results indicated that increasing the reinforcement ratio and using shear reinforcement enhanced the load-carrying capacity of the connections. However, increasing the percentage of the moment-to-shear ratio had a detrimental effect on the connection behavior. Additionally, increasing the concrete compressive strength while maintaining the same flexural reinforcement ratio slightly improved the connection behavior.

Investigating all the parameters that may affect the behavior of RC members in the lab is challenging due to constraints such as time, space, and funding, with the latter being particularly significant. Parameters such as the span-to-depth ratio or column–aspect ratio may require different formwork or significant changes to test setups for each specimen, which is often impractical in laboratory settings. Therefore, finite element (FE) software serves as a useful tool for exploring and studying the effects of these parameters on FRP-RC member behavior. However, robust experimental tests in the lab are still necessary as a starting point and foundation for the verification process required to evaluate the accuracy of any FE program before studying any parameter.

The aim of this essay is to understand part of the behavior of FRP-RC interior slab–column connections. The primary authors of the aforementioned projects collaborated to evaluate the effect of three parameters (perimeter-to-depth ratio, span-to-depth ratio, and column–aspect ratio) on the behavior of this type of connection.

2. Slabs Tested in the Lab

Four GFRP-RC specimens were cast in the laboratory, with their characteristics being outlined in the following sections [3].

All the slabs were square, with a side length of 2.5 m. Half of them had a thickness of 0.2 m, and the other half had a thickness of 0.35 m. A central column stub, with a cross-section of 0.3 m × 0.3 m, extended from the slab's top and bottom for 0.3 m. All the column stubs were provided with steel bars and stirrups to prevent any unexpected failure mode. Each specimen was named using three characters. The first character represented the longitudinal GFRP flexural reinforcement ("G"). The second and third characters indicated the specimen's thickness and flexural reinforcement ratio, respectively. The specimens were designed according to the recommendations of the Canadian standard for FRP-RC material [7]. The configuration for a typical specimen is illustrated in Figure 1. The mechanical properties of the reinforcement are documented in Table 1, and the properties for each specimen can be observed in Table 2.

Table 1. GFRP's bars.

Diameter, $Ø_f$ (mm)	Cross-Sectional Area, A_f (mm^2)	Failure Strength, f_{fu} (MPa)	Modulus of Elasticity, E_f (GPa)	Failure Strain, ε_{fu} (με)
20	284	765	48.1 ± 0.7	15,900
15	199	769	48.2 ± 0.4	15,950

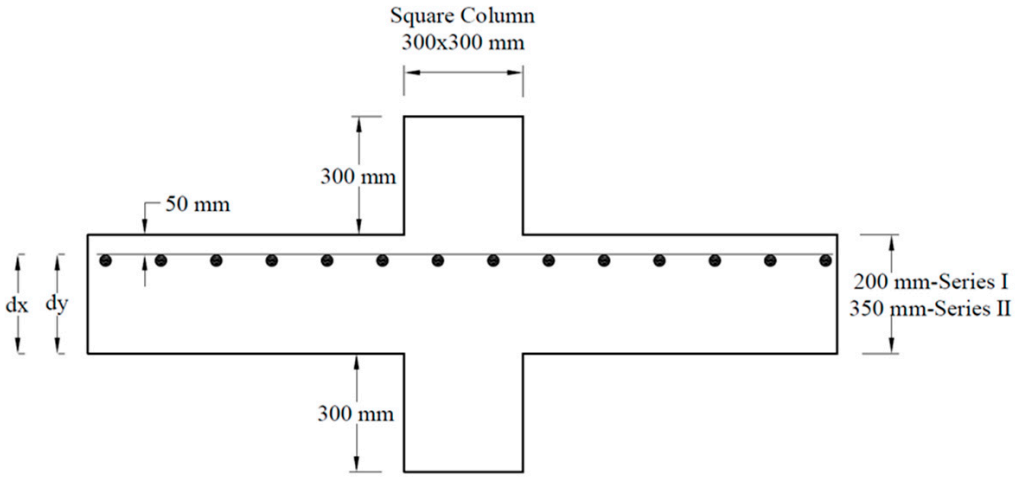

Figure 1. Typical specimen's overview.

Table 2. Details.

Slab ID	f_c' (MPa)	Thickness	Reinforcement		Failure Load V_{exp} (kN)	Reinforcement Strain (με)	FE Model Failure Load V_{Mod} (kN)	V_{exp}/V_{Mod}
		m	Longitudinal	ρ_f (%)				
G-0.20-0.70	34.3	0.20	12 No. 15	0.7	329	8975	325	1.01
G-0.20-1.60	38.6	0.20	18 No. 20	1.6	431	5010	427	1.01
G-0.35-0.30	34.3	0.35	12 No. 15	0.3	825	8190	852	0.97
G-0.35-0.70	39.4	0.35	18 No. 20	0.7	1071	4625	1056	1.01
Average					--	--	--	1.00
V_{exp}/V_{Model}					--	--	--	1.00
S.D (%)					--	--	--	1.70
COV (%)					--	--	--	1.70

2.1. Test Setup

The slabs were tested under the effect of pure shear force using a hydraulic jack. The applied load was recorded using a load cell connected to a computer. The load was applied from the bottom on the entire cross-section of the column stub, as depicted in Figure 2. The supporting frame consisted of four steel tubes placed on the top of the slab (tension side), with the distance between the centerlines of the tubes maintained constant in both orthogonal directions at a value of 2.0 m [3].

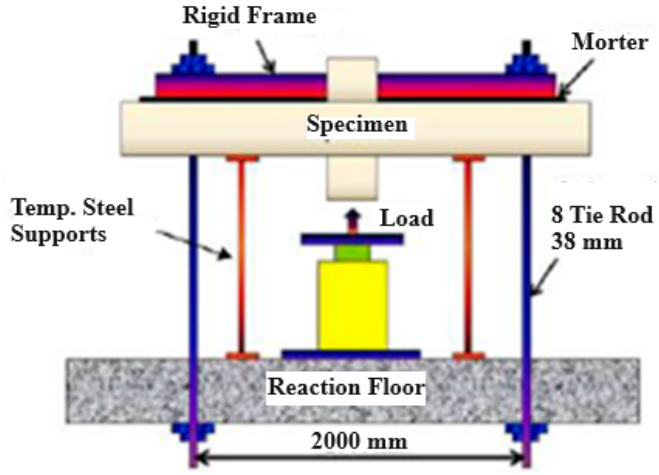

Figure 2. Three-dimensional test setup.

2.2. Major Results

The slabs failed in punching shear, with the column stubs penetrating through the slabs. The strains captured by the instruments were minimal until the formation of the first crack, after which, the strains began to increase exponentially. The observed strains in the reinforcement suggested that the failure of the specimens was not triggered by the rupture of the reinforcement, as the strains were well below the ultimate tensile strength of the GFRP bars, as evidenced in Tables 1 and 2 [3].

Increasing the reinforcement ratio by 120% from 0.7 to 1.6% enhanced the capacity of the specimen by 35% for the slabs with a 0.2 m thickness. This percentage enhanced to 80% when increasing the reinforcement ratio from 0.3 to 0.7% for the slabs with a 0.35 m thickness.

3. The Numerical Study

3.1. General

The various components employed in the numerical study to replicate the slabs that were tested in the lab are briefly described in the following sections.

3.2. Concrete

The algorithm model used in the current stage to simulate concrete elements is called *CC3DNonLinCementitious2* [8]. This model consists of two main groups of equations: the Menétrey–Willam model and the Rankine fracturing model. The latter accounts for the fracture behavior of the concrete elements, using the principal stresses and strains induced by external forces to simulate and depict the cracking pattern inside the concrete elements. The Menétrey–Willam model represents the failure surface that addresses the plastic behavior of the concrete elements.

The concrete stress–strain relation can be seen in Figure 3a. The relation comprises two main parts, compression and tension. In the uncracked compressive part, the algorithm recommended by the CEB-FIB Model Code [9] is followed. The equations used are suitable for all types of concrete according to the code. At the onset or after reaching the maximum compressive strength, the relation becomes a perfectively gradient descent line between the compressive stress and strain. In the uncracked tension part, the relation is linear up to the tensile strength of the concrete. Once cracks occur, the behavior is a downward curve that follows the relationship or the mathematical formulas of Hordijk [10].

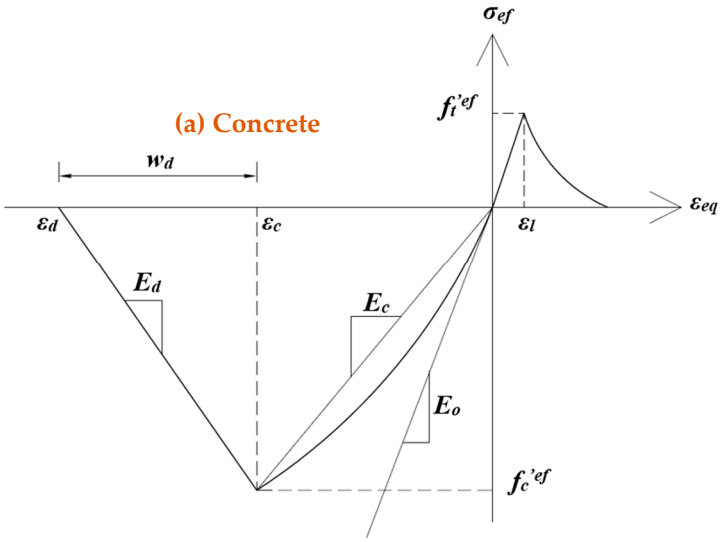

Figure 3. *Cont.*

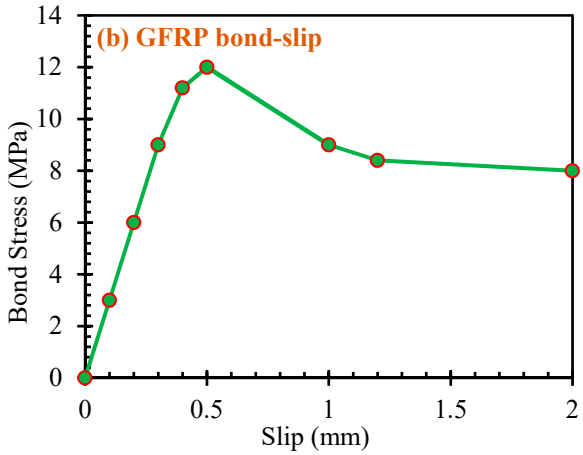

Figure 3. Stress–strain graphs: (**a**) concrete's stress–strain graph, reproduced from [8] and (**b**) FRP's bond–slip graph, reproduced from [11].

3.3. Reinforcement

The FE program considers and calculates the stiffness of the rebars and adds it to the overall stiffness of the concrete elements. The discrete method was used to model all the reinforcements, as this suits the casting of the slabs tested in the lab. In this method, the rebars are dealt with as link members with two nodes for each member that have three translational movements at each node.

It is well known that FRP materials behave linearly elastic up to failure. Therefore, to model the rebars, a linear stress–strain relation was used for the GFRP reinforcement, with the aid of the mechanical properties documented in Table 1, up to the maximum tensile strength of the rebars. From that point, an immediate drop in the tensile capacity of the rebars was considered to account for the rebars' rupture.

3.4. Bond Slippage Models

Usually, the bond stresses are distributed equally to some degree along the perimeter of any sand-coated rebar, which is the case with the GFRP rebars used in the slabs tested in the lab. In the current study, the contact stress between the rebar's parameter and the surrounding concrete was considered.

The relation between the stresses and slippage for the GFRP rebars is shown in Figure 3b. This relation was derived from tests that were performed in the lab [11], and it is an upward relation that is either straight or almost straight up to the ultimate bond stresses. From this point going further, the relation is a downward line followed by an almost flat plateau up to failure.

3.5. Solution Control

External forces are applied in the FE programs in an approach or way similar to that conducted in the lab. These forces are, often, applied at a constant rate and usually broken down into sequences of smaller steps. The program computes the stiffness following every step and this is known as the first iteration. At this point, internal stresses and strains are computed and generated inside the FE model to account for the effect of the applied load. The program then computes the difference between the applied load and the generated internal forces, and if this difference falls within the pre-created marginal limit, the program applies the next step and considers the previous computed stiffness as the initial one for the current step. If the previous step cannot be accomplished, the program will keep trying by assuming different internal forces until equilibrium is obtained. Nevertheless, if equilibrium is out of reach, the analysis will be terminated and that step will be considered the ultimate strength of the structure.

3.6. The FE Slabs

Figure 4 outlines a common FE slab. Multiple-sided polygons, such as octagons, were employed during modeling due to the complex shapes of the slabs, test setup, and boundary conditions. Selecting a suitable size for the FE mesh is an essential process, since it has a great consequence on the results. The suitable one was found to be 0.1 m; reducing it more than that did not impact the results in any way, and took undesired additional time to obtain the results. On the other hand, when the mesh size was greater than 0.1 m, the test results were rough and inexact. The concrete parameters were designated with the help of the compressive strength, as shown in Table 2.

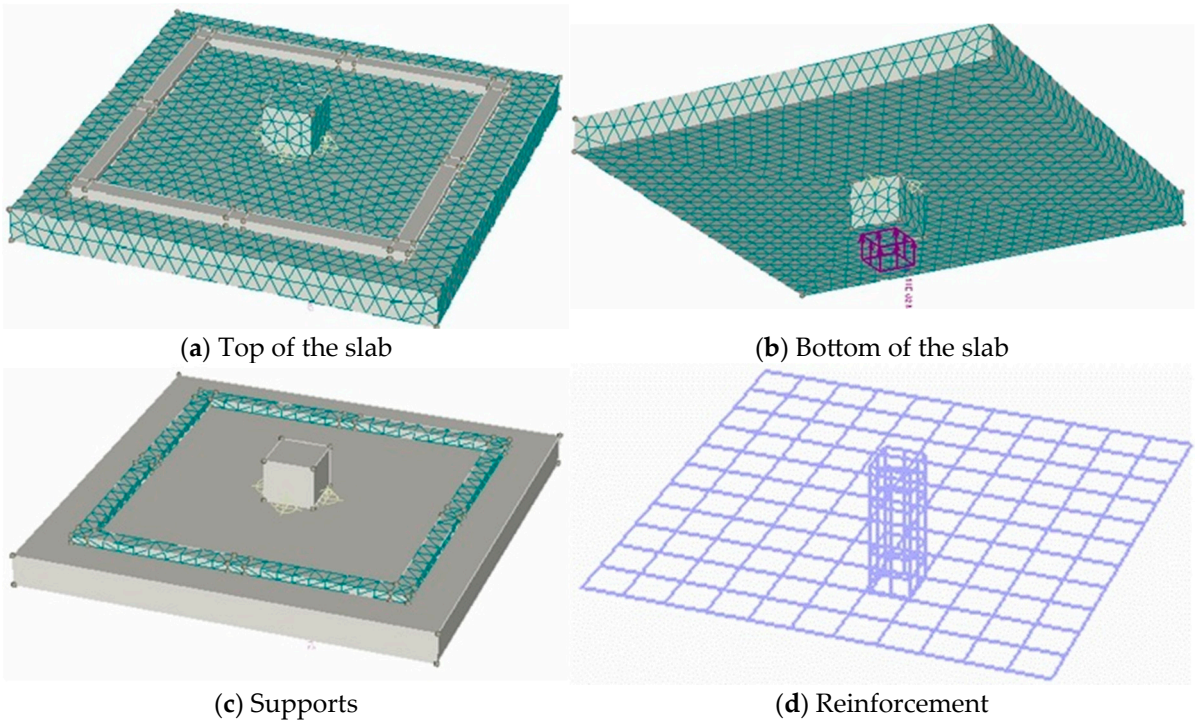

(**a**) Top of the slab (**b**) Bottom of the slab

(**c**) Supports (**d**) Reinforcement

Figure 4. Geometry of a typical slab.

To replicate the supporting conditions, four steel tubes were modeled and placed on the top side (tension side) of each slab at the appropriate locations. Similar to the tests that were performed in the lab, movements were prevented, in all directions, at the corners and middle of all the steel tubes. The applied shear force was 1 kN, for every step. The force was uniformly distributed along the surface of the bottom column stub acting in an upward direction.

To record the deformation of each slab, four monitoring points were placed on the tension side of the slab at 40 mm from the column face, two for each direction. Similarly, four were used to obtain the reinforcement strains at the column face.

3.7. The Verifying Step

Most of the time, and usually for slabs tested under pure shear force only, the first crack is an inclined crack connecting or starting from the edge or the corner of the column and heading toward the corner of the slab. The width and severity of these cracks increase as the shear force increases. The first circular crack around the column commonly appears at or around fifty percent of the ultimate shear force. At failure, and especially for slabs without shear reinforcement, the column punches through the slab with the concrete's cover for the reinforcement, being taken off. Figure 5 outlines the cracks' schematic of G-0.2-1.6 tested in the lab as an example, and the FE model of that slab. As evidenced in the figure, the FE model was able to copy the cracks' schematic to a perfect degree.

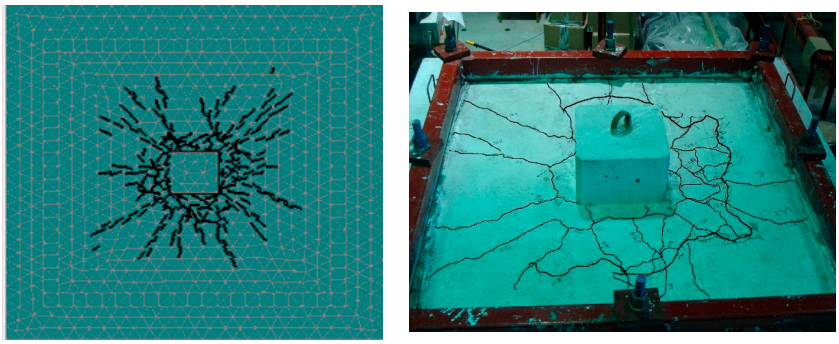

(**a**) (**b**)

Figure 5. Cracks' schematic (tension side). (**a**) FE slab; (**b**) Experimental [3].

Before cracking, the full cross-section of the slab resists the applied shear force, therefore, the slab's displacement is not that significant and the load–deflection relationship is nearly linear. After the development of the cracks, the stiffness decreases and, again, the load–deflection relation is a line but with a lesser slope. Between the previous two stages, usually, there is a smooth transitional curve that connects the two lines together. The deflection captured at 40 mm from the column face in relation to the shear force for the slabs tested in the lab and the ones made with the FE program followed the previous mentioned trend, as seen in Figure 6. The close proximity of the deflection recorded by the FE program to the slabs tested in the lab can be seen in the figure as well.

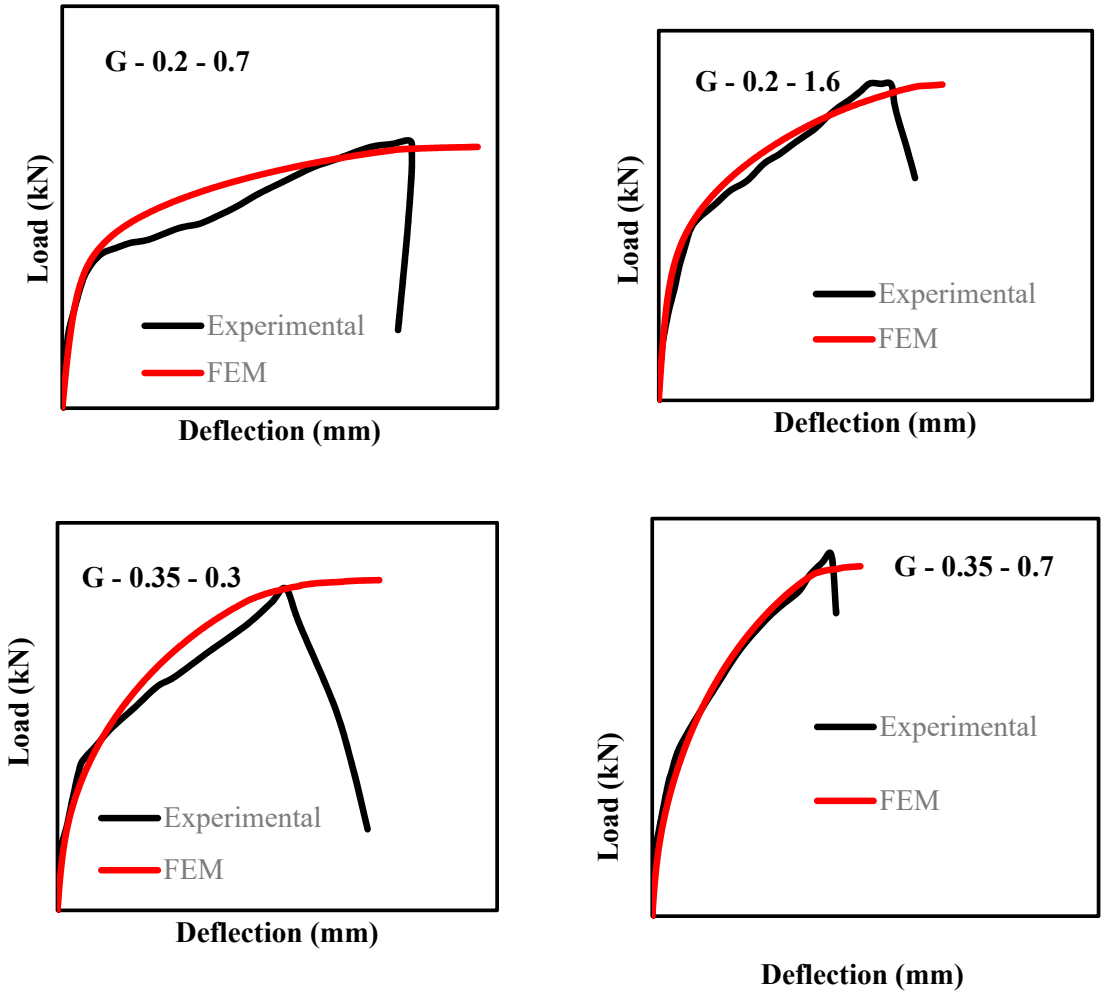

Figure 6. Load–deflection at 40 mm from the column face.

The tensile strain for the reinforced bar located at the column face against the shear-force is shown in Figure 7 for all four slabs and their FE equivalents. The figure clearly shows the closeness of the strains imitated by the FE models to the ones investigated in the lab. The previous observation is noticeable in the pre-cracking as well as the post-cracking behavior of the slabs.

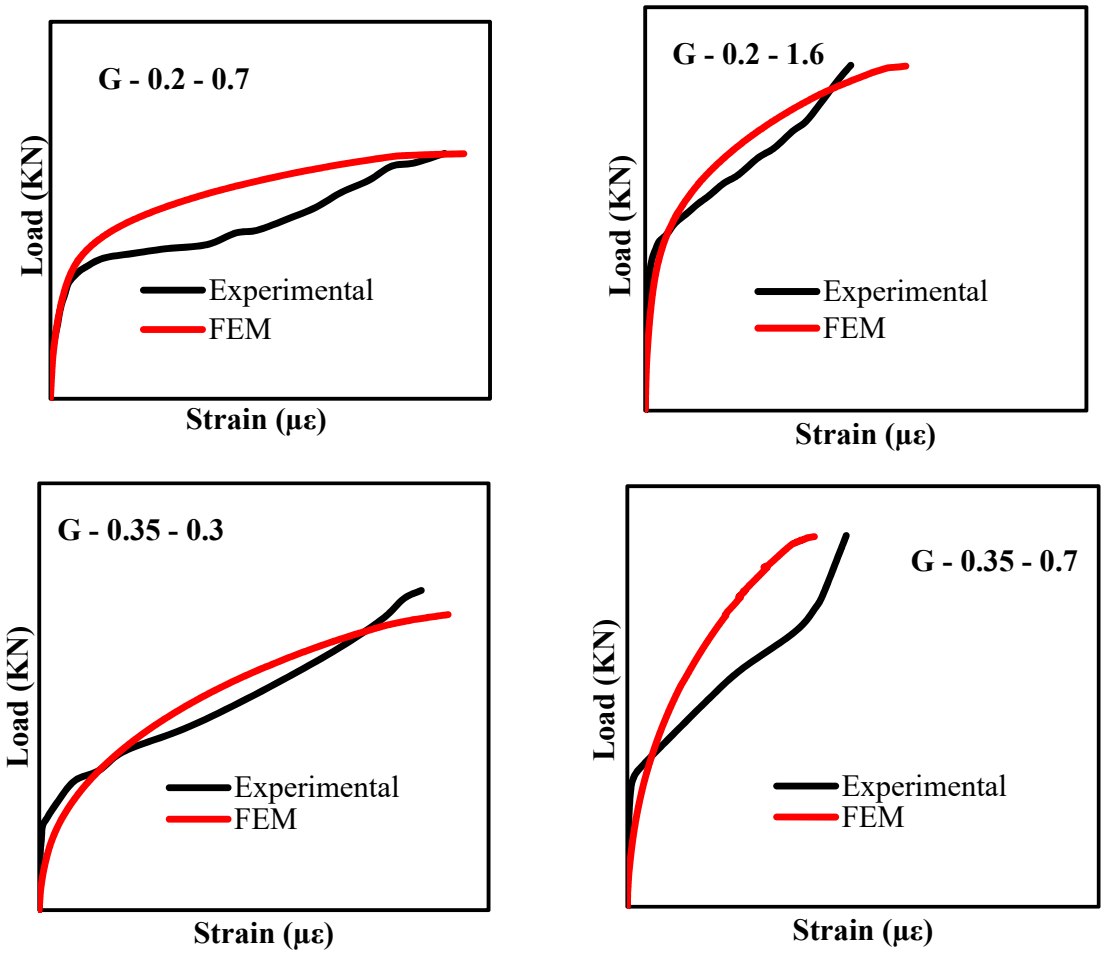

Figure 7. Load–reinforcement strains at the column face.

The ultimate shear force of the slabs from the experimental tests and the FE program is given in Table 2. The numerical numbers are within 3%, at the most, from the ones acquired experimentally. The average ratio between the experimental and the numerical shear force (V_{exp}/V_{Model}) for all the slabs is "1.00 ± 0.02", accompanied by 1.7% COV.

The above results show, beyond a doubt, the effectiveness of the FE method in mimicking the behavior of the RC slabs.

3.8. The Parametric Step

The properties of G-0.2-1.6 were the foundation of the current step. Fifteen slabs were built to study the effect of the following three parameters on the behavior of FRP-RC interior slab–column connections.

1—Column–aspect ratio. Five slabs with different column cross-sections (0.3 × 0.3-m, 0.3 × 0.6 m, 0.3 × 0.9 m, 0.3 × 1.2 m, and 0.3 × 1.5-m) were created to have ratios of 1.0, 2.0, 3.0, 4.0, and 5.0, respectively. The dimensions of the slabs and the positions of the supports were altered for each prototype to eliminate the effect and maintain a constant value equal to six of the span-to-depth ratio.

2—Perimeter-to-depth ratio for a square column stub. The side length for the column was between 0.3 and 0.7 m, with a 0.1 m increment. The average depth was kept constant at 0.13 m. The ratios for the tested slabs were 13, 16, 19, 22, and 25.

3—Span-to-depth ratio, from four to twelve, with an equal increment of two.

The name of each slab had four segments. The first was "G", since all the slabs were reinforced with GFRP bars. The following was a number to define the column–aspect ratio. The third was also a number for the smaller dimension of the column cross-section. The last one was for the ratio between the clear span from the column face up to the support divided by the effective slab's depth.

3.8.1. Column–Aspect Ratio

The shear force against the deformability, measured at 40 mm from the column face in the direction of the smaller dimension of the column, is depicted in Figure 8a. Slab G-1-0.3-6 had the highest deformability among those examined in the current parameter. Increasing the column–aspect ratio increased the column's circumference, and subsequently, the shear stresses were spread out in longer distances, and that was the direct reason for the enhancement and reduction in the slabs' deformability. The above behavior can be seen in the figure, as the deformability was reduced by 37, 57, 68, and 76% for G-2-0.3-6, G-3-0.3-6, G-4-0.3-6, and G-5-0.3-6, opposite to G-1-0.3-6, sequentially, at the same shear level. The same behavior was noticeable for the post-cracking flexural stiffness, calculated as the average percentage between the shear force and the deformability, where the reductions were 2, 10, 16, and 22%.

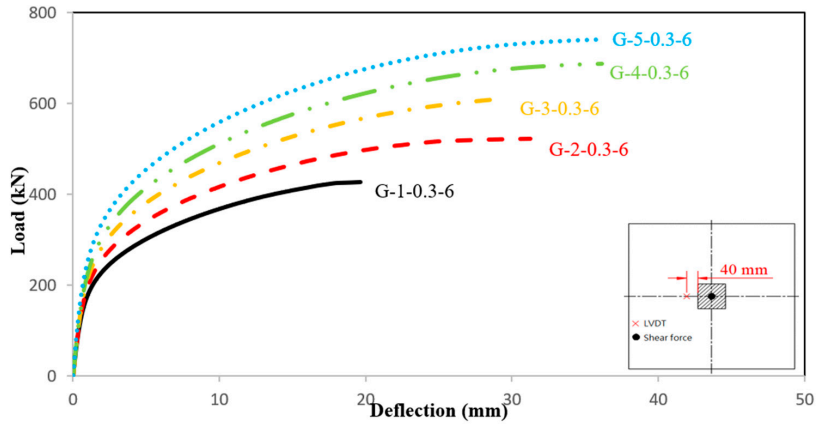

(**a**) Slabs with different column–aspect ratios

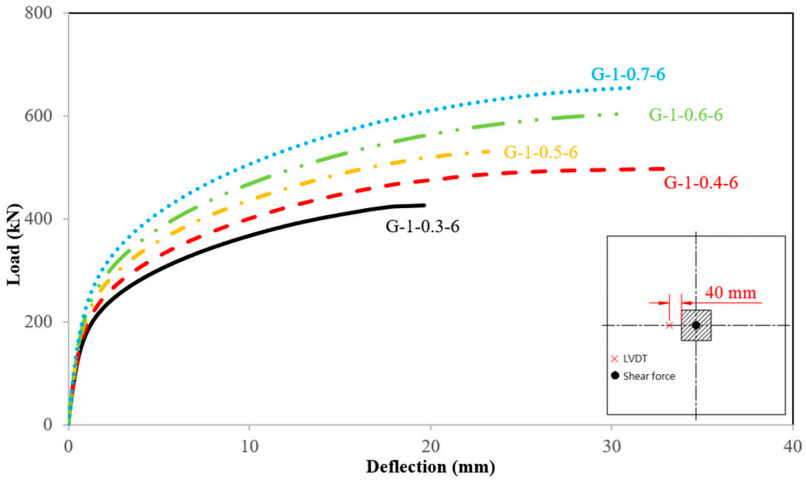

(**b**) Slabs with different perimeter-to-depth ratios

Figure 8. *Cont.*

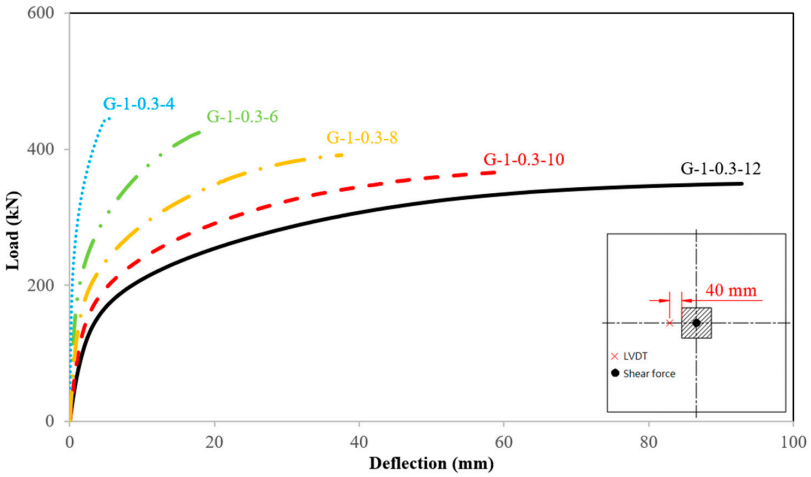

(**c**) Slabs with different span-to-depth ratios

Figure 8. Load verses displacement.

According to the serviceability limit states in the North American codes for FRP-RC material [7,12], one of the factors that might control the design of FRP-RC elements is the curvature of the structure. Due to the elastic behavior and low modulus of elasticity of FRP bars, FRP-RC members would exhibit larger deflections with respect to members reinforced with steel bars. Therefore, it is paramount to try to find a way or a formula to capture the curvature of these FRP-RC members, especially after cracking. The post-cracking stiffness is directly related to the increase in the column–aspect ratio, as depicted in Figure 9. The relation between the stiffness and the column–aspect ratio is shown in Equation (1). This equation would help designers in obtaining the value of the deflection at any shear level after cracking by computing the flexural stiffness first from Equation (1).

$$Kp = 0.032\ (0.5931\beta_c + 9.649)\left(E_f\ \rho_f\ f'_c\right)^{\frac{1}{3}} \quad (1)$$

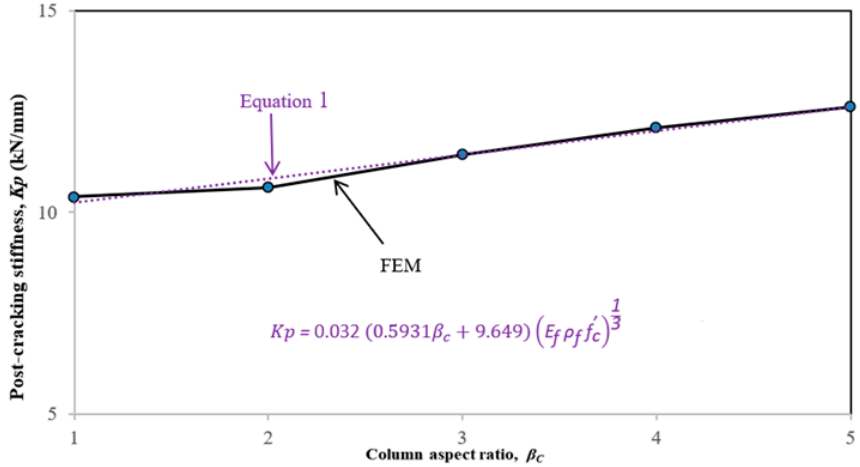

Figure 9. Post-cracking stiffness verses column–aspect ratio.

The strains captured in the GFRP reinforcement at the column face against the shear force are shown in Figure 10a. Before the cracks commenced in the slabs, the differences in the captured tensile strains were not intelligible and the strains elevated exponentially at the onset of the cracking stage. The ultimately observed tensile strains in G-1-0.3-6, G-2-0.3-6, G-3-0.3-6, G-4-0.3-6, and G-5-0.3-6 were 5910, 5010, 4540, 4680, and 4700 με, sequentially, and accounted for 37, 31.5, 28.5, 29, and 29.5% of the rupture's strains of the used GFRP bars. That suggests that no failure occurred or was observed in the GFRP bars

at failure. Slab G-1-0.3-6 had the highest captured strains. At a similar level for the shear force, G-2-0.3-6, G-3-0.3-6, G-4-0.3-6, and G-5-0.3-6 had less strain by 57, 74, 83, and 86% with reference to G-1-0.3-6, sequentially, and the enhancement at failure was 15, 23, 21, and 20%.

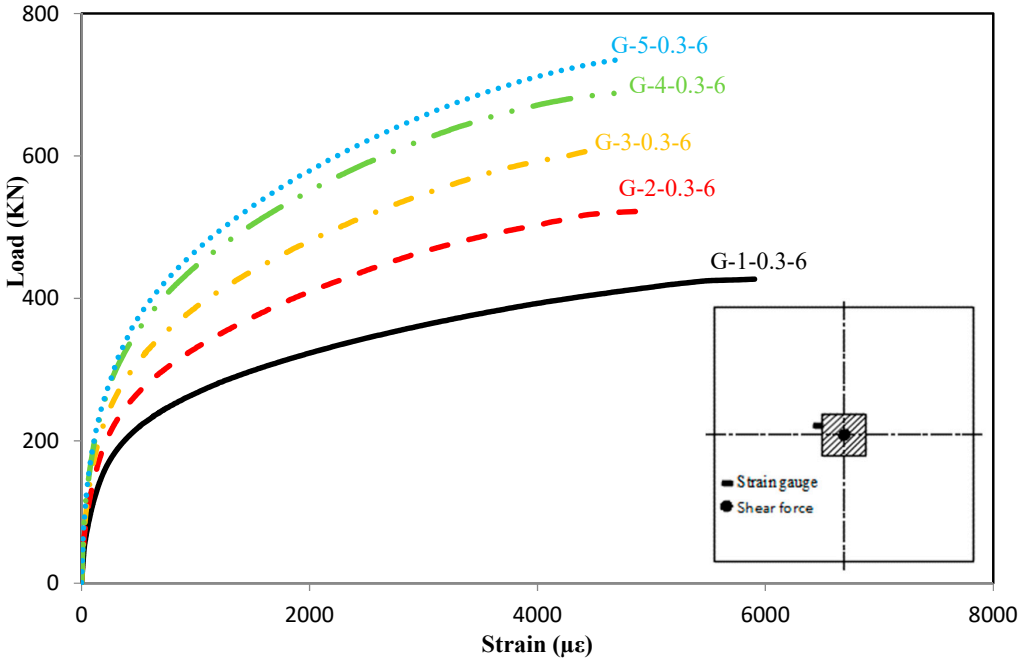

(**a**) Slabs with different column–aspect ratios

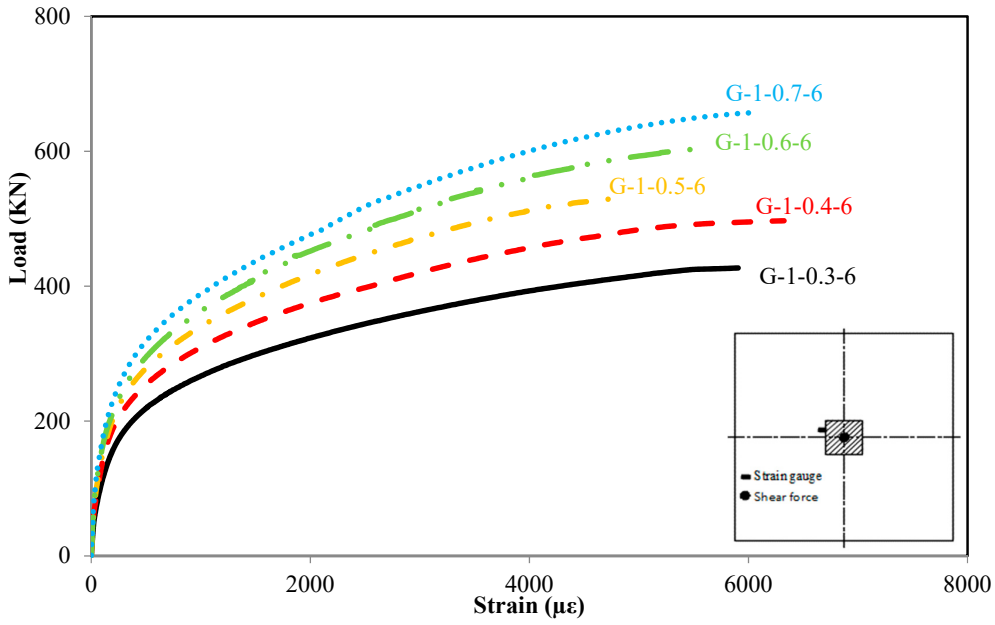

(**b**) Slabs with different perimeter-to-depth ratios

Figure 10. *Cont.*

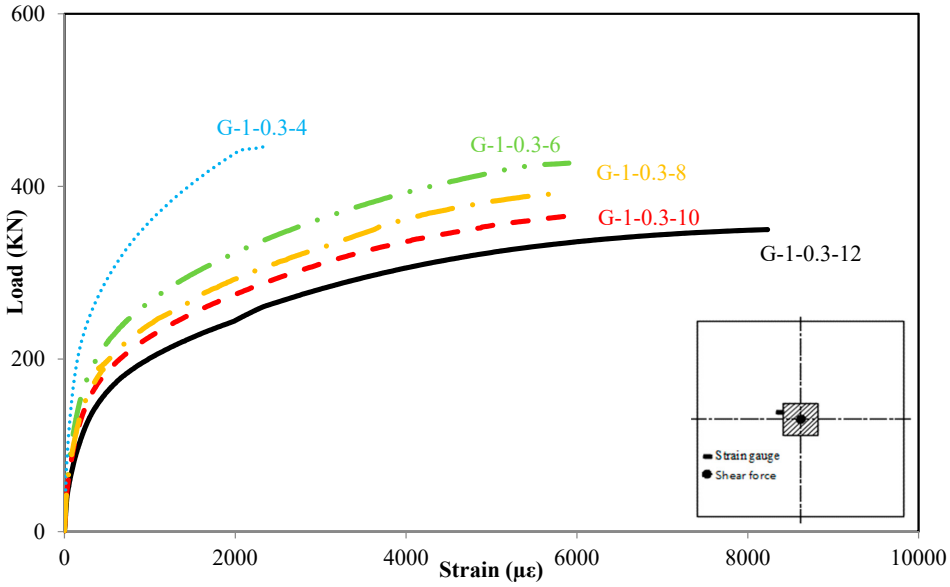

(**c**) Slabs with different span-to-depth ratios

Figure 10. Load verses strain in the longitudinal reinforcement.

The punching shear stresses calculated at half the average depth from the column face, 0.5*d*, are shown in Table 3. Increasing the column–aspect ratio reduced the ultimate shear stresses. The decreases for G-2-0.3-6, G-3-0.3-6, G-4-0.3-6, and G-5-0.3-6 were around 9, 16, 23.5, and 27% with reference to G-1-0.3-6, sequentially.

Table 3. Results of the numerical study.

Slab's Designation	Shear Force V_{Mod} (kN)	Failure Shear Stress (v_c) (MPa)	Failure Strain (με) Bars	Ultimate Mid Deflection (mm)
Series I: Column–Aspect Ratio				
G-1-0.3-6	427	1.91	5910	19.6
G-2-0.3-6	523	1.73	5010	31.2
G-3-0.3-6	610	1.61	4540	29.4
G-4-0.3-6	668	1.46	4680	36.1
G-5-0.3-6	746	1.39	4700	35.8
Series II: Perimeter-to-Depth Ratio				
G-1-0.3-6	427	1.91	5910	19.6
G-1-0.4-6	497	1.80	6320	33.3
G-1-0.5-6	531	1.62	4850	23.2
G-1-0.6-6	605	1.59	5630	31.1
G-1-0.7-6	663	1.54	6010	31.3
Series III: Span-to-Depth Ratio				
G-1-0.3-4	447	2.00	2370	5.57
G-1-0.3-6	427	1.91	5910	19.6
G-1-0.3-8	392	1.75	4900	26.9
G-1-0.3-10	366	1.64	5930	58.8
G-1-0.3-12	350	1.56	8230	92.8

To have a constant ratio of 13 between the perimeter (1.72 m), measured at 0.5*d* from the column face, to the depth (0.13 m), while having different column–aspect ratios, five more slabs with different column dimensions of 0.3 × 0.3 m, 0.4 × 0.2 m, 0.45 × 0.15 m, 0.48 × 0.12 m, and 0.5 × 0.1 m were built to have column–aspect ratios of 1.0, 2.0, 3.0, 4.0, and 5.0, respectively. The dimensions and supports' locations for each slab were changed

to have span-to-depth ratio of six. The shear stresses calculated at 0.5 *d* were reduced by 18, 23, and 43% from 1.91 to 1.56, 1.46, and 1.08 MPa, for increasing the aspect ratio by 100, 200, and 300%, respectively. Increasing the column–aspect ratio from 4.0 to 5.0, however, increased the shear stresses by 5.5% from 1.08 to 1.14 MPa. These results are, somewhat, in good agreement with the literature [13]. The researchers in that report studied the effect of the column–aspect ratio on interior slabs reinforced with steel bars. The test results showed that the punching shear stress decreased up to a column–aspect ratio equal to three, then it increased after that. The authors [13] concluded that the effect of the column–aspect ratio faded after a value equal to three.

3.8.2. Perimeter-to-Depth Ratio

The shear force and the deflection obtained at 40 mm from the column face are shown in Figure 8b for the slabs with different perimeter-to-depth ratios. It was kept in mind that, for the five slabs tested, the span-to-depth value was kept constant at a value of six by slightly changing the dimensions of the slabs to accommodate for that. Generally speaking, the behavior of the slabs was not that different from that brought up beforehand with the "column–aspect ratio" part. As expected, the slab with a perimeter-to-depth ratio equal to 13, G-1-0.3-6, had the least shear force and shear stiffness. Weighing up the deflection of the slabs at the same shear level showed an enhancement or drooping by 27, 46, 57, and 67% when increasing the perimeter-to-depth ratios by 33, 66, 100, and 133%, sequentially. The same can be said for the post-cracking stiffness, where G-1-0.4-6, G-1-0.5-6, G-1-0.6-6, and G-1-0.7-6 had a higher stiffness by 11, 22, 48, and 101%, respectively, in relation to G-1-0.3-6. The figure also shows that at or close to the failure stage, a flat plateau seemed to be the trend in the load–defection relationship, which indicates a higher increase in the deformability of the slabs with any small change in the value of the shear force due to the high deterioration of the stiffness.

The shear force versus the tensile strains in the GFRP bar located at the column face can be found in Figure 10b for the slabs with different perimeter-to-depth ratios. This behavior was also pretty close to that reported in the "column–aspect ratio" portion. Increasing the perimeter-to-depth ratio positively affected the strains at the same shear level. Slabs G-1-0.4-6, G-1-0.5-6, G-1-0.6-6, and G-1-0.7-6 had less strains by 40, 59, 68, and 74%, respectively, in relation to G-1-0.3-6. The highest reordered strain in this group was 6320 micro-strains, which is well below the rupture strains of the GFRP bars used, as shown in Table 1. These results suggest that the slabs in this group failed in shear, not in flexure, or at least at the time of failure, no rupture was observed in the GFRP bars.

Increasing the dimensions for the square column stub will increase the perimeter that withstands the shear force. That will, consequentially, reduce the punching shear stresses. Table 3 shows the punching shear stresses calculated at 65 mm from the column face, 0.5*d*. Slabs G-1-0.4-6, G-1-0.5-6, G-1-0.6-6, and G-1-0.7-6 had less shear stresses by 6, 15, 17, and 19% in comparison with G-1-0.3-6. To study the combined effects of the perimeter-to-depth ratio and span-to-depth ratio, five more slabs were created based on the dimensions and supports' locations of G-1-0.3-6. The only difference between these five slabs was the dimensions of the square column stub. The results showed that increasing the side length of the column from 0.3 to 0.6 m with a 0.1 m increment reduced the stresses by 4, 5, and 10% from 1.91 to 1.83, 1.82, and 1.72 MPa. However, similar to that reported in the pervious section, increasing the column dimensions from 0.6 to 0.7 m increased the shear stresses by 2.3% from 1.72 to 1.76 MPa. Many researchers have reported similar results, increasing the dimensions of the square column stub by 50%, from 0.3 to 0.45 m, for slabs reinforced with GFRP bars and tested under the effects of shear force and unbalanced moment, and reducing the shear stresses by 29% [14]. For slabs reinforced with steel bars, increasing the perimeter-to-depth ratio for eccentrically loaded edge slab–column connections by 69% from 6.5 to 11 lowers the shear stresses by roughly 20% [15]. The authors of the current article strongly recommend not taking the results from the literature assuming that this was only due to an increase in the perimeter-to-depth ratio, as many of the results mentioned

in the literature were actually due to the combined effects of the perimeter-to-depth ratio and span-to-depth ratio. For instance, increasing the perimeter-to-depth ratio in interior slabs reinforced with steel bars by 25% (from 13.3 to 16.6) decreased the shear stresses by 10% [16]. According to the report, the only difference between the slabs was the side length of the square column stub (0.22 and 0.3 m).

3.8.3. Span-to-Depth Ratio

Five slabs were built based on the geometry and material properties of G-1-0.3-6, and the only difference between the slabs was the span-to-depth ratio. Decreasing the span-to-depth ratio had a high, distinct, and detectable impact on the slabs' curvature. The post-cracking rigidity increased significantly, and the slabs experienced less deflection, as shown in Figure 8c. Slabs G-1-0.3-10, G-1-0.3-8, G-1-0.3-6, and G-1-0.3-4 had less deflection at the same shear level by 38, 69, 86, and 97%, in indication to the one with the higher span-to-depth ratio, G-1-0.3-12. At failure, these numbers became 37, 60, 79, and 94%. The increase in the post-cracking rigidity was 56, 104, 191, and 777% from 3.5 to 5.5, 7.3, 10.4, and 31.25 kN/mm. It can be noticed in the figure that increasing the span-to-depth ratio also increased the non-linearity, as the relation tended to be approximately flat at the failure stage.

The beam or the one-way slab's action is the controlled way of behaving for slabs with high span-to-depth ratios. As the span-to-depth ratio decreases, the arch's action begins to contribute or become the controlling mode for the slabs' behavior, where part of the shear force transfers through somewhat direct routes to the supports, in forms of triangular shapes, through compressive struts and tensile ties. The compressive struts are generated within the parts of the uncracked concrete, and they run between the shear force and the supports. The GFRP longitudinal reinforced bars will be the ties that connect these supports together. Based on the previous explanations, the strains should be reduced as the span-to-depth ratio increases. Slabs G-1-0.3-10, G-1-0.3-8, G-1-0.3-6, and G-1-0.3-4 had less strains at the same shear level by 28, 42, 59, and 85% in comparison to G-1-0.3-12, respectively. These percentages were 28, 30, 28, and 71% at failure.

Previous published works categorized reinforced members into two groups. The first is called long members for a span-to-depth ratio of greater than 2.0, and the second is short or deep members for a span-to-depth ratio of less than 2.0. As an established rule, as the span-to-depth ratio decreases, the strength of the member increases. This improvement is more noticeable in deep members, as a large portion of the shear force transmits to the supports. Slabs G-1-0.3-10, G-1-0.3-8, G-1-0.3-6, and G-1-0.3-4 had a higher shear strength by 5, 12, 22, and 28% in comparison to G-1-0.3-12, respectively. The effect of the span-to-depth ratio on steel-RC slabs with values equal to 2, 4, 6, 8, and 12 was analyzed [17]. The reported results showed an increase in the punching shear stresses as the ratio went below 6, which agrees with results reported herein. Comparing the results with the available design code at that time [18] showed a high underestimation for the actual punching shear stresses, especially with the slabs that had a small span-to-depth ratio.

3.9. Punching Shear Values According to the FRP-RC Standards

The Canadian standard [7] recommends using three equations (Equations (2)–(4)) to calculate the punching shear strength of slabs reinforced with FRP bars. From the three equations, the minimum shear strength obtained should be used to calculate the safe value for the shear force.

$$v_c = 0.028\,\lambda\,\varphi_c\left(1+\frac{2}{\beta_c}\right)\left(E_f\,\rho_f\,f'_c\right)^{\frac{1}{3}} \quad \text{(MPa)} \tag{2}$$

$$v_c = 0.147\,\lambda\,\varphi_c\left(0.19+\alpha_s\frac{d}{b_0}\right)\left(E_f\,\rho_f\,f'_c\right)^{\frac{1}{3}} \quad \text{(MPa)} \tag{3}$$

$$v_c = 0.056\,\lambda\,\varphi_c\left(E_f\,\rho_f\,f'_c\right)^{\frac{1}{3}} \quad \text{(MPa)} \tag{4}$$

Unlike the Canadian standard, the American standard [12] has only one main Equation (5) for calculating the punching shear force of slabs reinforced with FRP bars.

$$V = \frac{4}{5}\sqrt{f'_c}\;b_0\,c\;\text{(N)} \tag{5}$$

where $c = kd$ (mm)

$$k = \sqrt{2\rho_f n_f + \left(\rho_f n_f\right)^2} - \rho_f n_f$$

The equation is based on a mathematical work [19]. According to the article, all the experimental work that was conducted on FRP-RC slab–column connections up to that date was collected and mathematical efforts were undertaken to come up with Equation (5), which was adapted from 2006 by the ACI committee 440 [20]. The code considers only five items in relation to the punching shear capacity of the slab–column connections: the effect of the column's perimeter, concrete compressive strength, reinforcement ratio, elastic modulus of the reinforcement, and concrete in the factor called n_f.

The Japanese Standard [21] also has one equation to calculate the carrying shear capacity of slab–column connections (Equation (6)).

$$v_c = \beta_d\beta_p\beta_r f_{pcd} \tag{6}$$

$$\beta_d = (1000/d)^{1/4} \le 1.5$$

$$\beta p = (100\rho_f\,E_f/E_S)1/3 \le 1.5$$

$$\beta_r = 1 + \frac{1}{1 + 0.25u/d}$$

$$f_{pcd} = 0.2\sqrt{f'_c} \le 1.2$$

The Japanese Standard also takes five factors into consideration, which are the slab's depth, reinforcement ratio, elastic modulus of the reinforcement, column's perimeter, and the concrete compressive strength.

Table 4 and Figure 11 show all the predictions from the codes. Please keep in mind that the safety and material factors in all the standards were set as equal to one, not the recommended values by these codes.

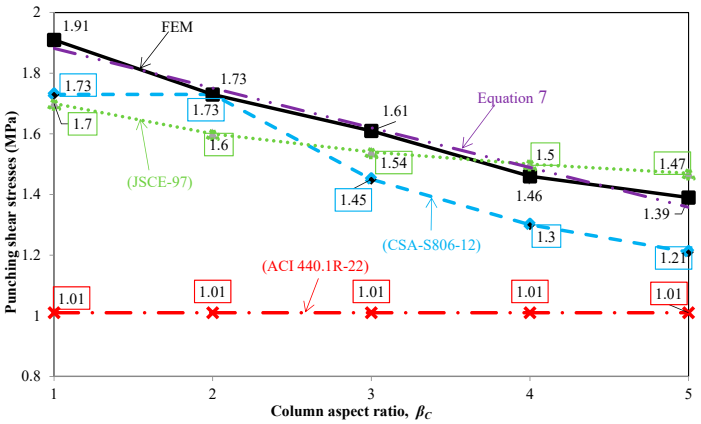

(**a**) Slabs with different column–aspect ratios

Figure 11. *Cont.*

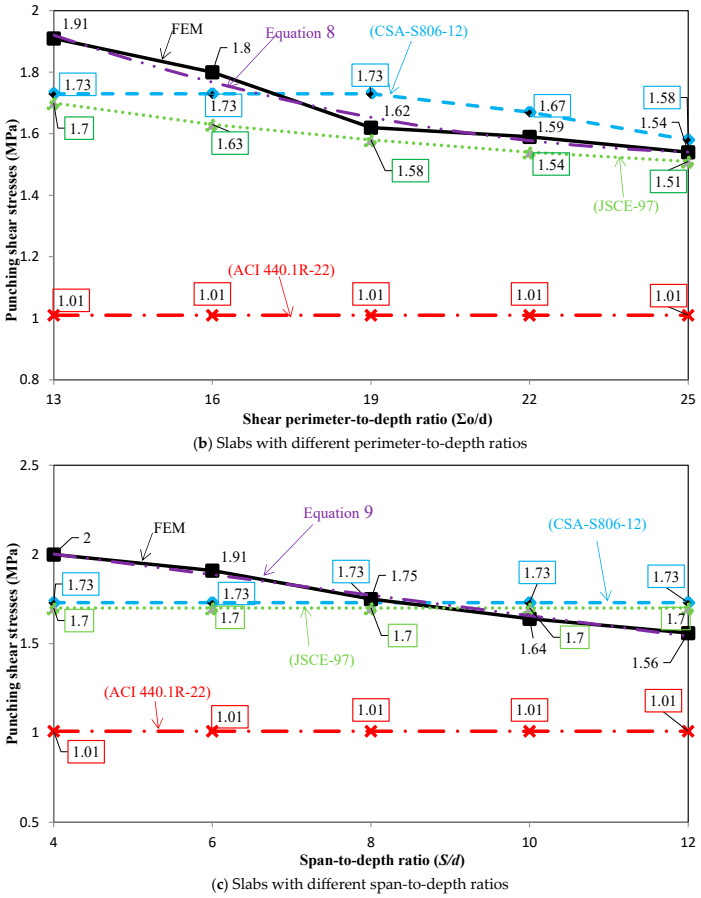

Figure 11. Punching shear stresses.

For the effect of the column–aspect ratio, the American code [12] gave constant predictions for all the slabs with a value equal to 1.01 MPa. The Canadian standard [7] was somewhat closer up to the column–aspect ratio equal to two, and after that, it tended to underestimate the shear stresses. For the Japanese code [21], the predictions were not totally accurate up to a column–aspect ratio equal to two. After that, the predictions were much better. The middle percentage for V_{mod}/V_{CSA} was 1.1 ± 0.07 with 0.05 COV.

These numbers were 1.03 ± 0.09 with 0.06 COV for the Japanese code [21] and 1.6 ± 0.25 with 0.11 COV for the American code [12]. Equation (7) shown in the figure is a mathematical effort to predict the shear strength due to the effect of the column–aspect ratio. The figure shows that the equation gave the closest prediction to the results.

$$v_c = 4.2 \times 10^{-3} \lambda \, \varphi_c \, (15.4 - \beta_c) \left(E_f \, \rho_f \, f'_c \right)^{\frac{1}{3}} \quad (7)$$

For the effect of the perimeter-to-depth ratio, again, the American code [12] failed to predict the punching stresses accurately, and the code gave constant predictions for all the slabs with a value equal to 1.01 MPa. The Canadian standard [7] was much better, however, the code did not consider the reduction in the stresses up to a perimeter-to-depth ratio approximately equal to 19. The Japanese code [21] gave somewhat better results for a perimeter-to-depth ratio between 19 and 25. Nevertheless, the code underestimated the shear stresses for a ratio between 13 and 19. The percentage for V_{mod}/V_{CSA} was 1.0 ± 0.08 with 0.06 COV. The percentage for the Japanese code [21] was 1.06 ± 0.05 with 0.04 COV, and for the American guidelines [12], was 1.67 ± 0.18 with 0.08 COV. Another Equation (8), is presented in Figure 11b to predict the stresses due to the effect of the perimeter-to-depth ratio. The equation gave better and closer results than those adapted by the three standards presented in the current article, as shown in the figure.

Table 4. Code predictions.

Slabs	The Canadia Code Predictions [7]		The American Code Predictions [12]		The Japanese Code Predictions [21]	
	$v_{CSA.}$ (kN)	$v_{mod.}/v_{CSA.}$	$v_{ACI.}$ (kN)	$v_{mod.}/v_{ACI.}$	$v_{JSCE1997.}$ (kN)	$v_{mod.}/v_{JSCE1997.}$
Series I: Column–Aspect Ratio						
G-1-0.3-6	387.8	1.10	226.5	1.88	380.1	1.12
G-2-0.3-6	521.8	1.00	305.6	1.71	483.4	1.08
G-3-0.3-6	546.6	1.11	384.6	1.58	585.4	1.04
G-4-0.3-6	595.2	1.12	463.6	1.44	687.6	0.97
G-5-0.3-6	650.2	1.15	542.6	1.37	789.7	0.94
Series II: Perimeter-to-Depth Ratio						
G-1-0.3-6	387.8	1.10	226.5	1.88	380.1	1.12
G-1-0.4-6	476.8	1.04	279.2	1.78	449.3	1.11
G-1-0.5-6	566.7	0.94	331.9	1.60	517.4	1.03
G-1-0.6-6	636.1	0.95	384.6	1.57	585.4	1.03
G-1-0.7-6	681.1	0.97	437.3	1.52	653.5	1.01
Series III: Span-to-Depth Ratio						
G-1-0.3-4	387.8	1.15	226.5	1.97	380.1	1.18
G-1-0.3-6	387.8	1.10	226.5	1.88	380.1	1.12
G-1-0.3-8	387.8	1.01	226.5	1.73	380.1	1.03
G-1-0.3-10	387.8	0.94	226.5	1.61	380.1	0.96
G-1-0.3-12	387.8	0.90	226.5	1.54	380.1	0.92

$$v_c = 6.4 \times 10^{-5} \lambda \, \varphi_c \left((\Sigma o/d)^2 - 55(\Sigma o/d) + 1500 \right) \left(E_f \, \rho_f \, f'_c \right)^{\frac{1}{3}} \quad (8)$$

All the codes failed to predict the reduction in the shear stresses associated with an increase in the span-to-depth ratio. However, the Canadian and Japanese ones [7,21] were still closer as opposed to the American guidelines [12]. The middle percentage for the Canadian standard was 1.02 ± 0.12 with 0.09 COV. For the Japanese code [21], the percentage was 1.04 ± 0.13 with 0.09 COV. For the American code [12], the percentage was 1.75 ± 0.21 with 0.09 COV. Equation (9) is presented:

$$v_c = 1.85 \times 10^{-3} \, \lambda \, \varphi_c \, (39 - (S/d)) \left(E_f \, \rho_f \, f'_c \right)^{\frac{1}{3}} \quad (9)$$

This in order to overcome the obvious shortcomings of the North American and Japanese standards in accurately predicting the punching shear stresses due to changes in the span-to-depth ratio.

3.10. Available Literature

Appendix A (Table A1) displays the available literature for interior and edge slab–column connections. According to the data and when compared to the three standards described here, the predictions from the three proposed Equations (7)–(9) are more accurate in predicting the actual punching shear strength of the connections. According to the proposed equations, the average values of the actual to predicted strength for the interior and edge slab–column connections are 1.11 and 1.1, sequentially. The Canadian standard [7] ratios are 1.2 and 1.22. The figures for the American guidelines [12] are 2.18 and 2.08. The percentages for the Japanese code [21] are 1.19 and 1.20.

4. Conclusions

Twenty-five slabs were discussed herein. This study offers new insights into the punching shear behavior in FRP-RC structures, highlighting the key influence of parameters like the column–aspect ratio, perimeter-to-depth ratio, and their interaction with the span-to-depth ratio, which no researcher has explored before. Equations (7)–(9) provide more accurate predictions than the current standards. However, limitations exist, including variability in the experimental setups. Future research should validate these equations across diverse structural configurations and loading conditions, guiding potential revisions and enhancing their practical applicability in engineering design. The following conclusions from the main findings are summarized:

1. Increasing either the column–aspect ratio or the perimeter-to-depth ratio leads to a reduction in the punching shear stresses, curvature, and captured strains. However, the combined effect of these factors with the span-to-depth ratio can yield varied outcomes, influenced by factors such as the test setup and support locations. Moreover, increasing the span-to-depth ratio decreases the shear stresses, while notably increasing the curvature and strains, particularly at failure.
2. The American code for FRP-RC materials [12] requires substantial revision. Based on the findings of this study, it is not recommended for use, as its current version significantly underestimates the punching shear capacity of slabs. The equation provided in the code relies on outdated research, highlighting the need for comprehensive updates.
3. The Canadian code for FRP-RC materials [7] offers three equations for predicting the punching shear capacity of slabs. While it performs better than the American guidelines [12] in predicting slab strength, further revisions are necessary, particularly to incorporate the influence of the span-to-depth ratio.
4. Despite being older than its American counterpart, the Japanese code for FRP-RC materials [21] provides more accurate results compared to the American guidelines [12]. However, there is room for improvement, especially concerning the consideration of the span-to-depth ratio in its predictions.

5. This study presents three equations (Equations (7)–(9)) to estimate the punching shear stresses in FRP-RC slabs. These equations offer more accurate predictions for the strength of interior and edge slab–column connections compared to the standards discussed.
6. Based on the data and discussion outlined in the article, it seems that this behavior is primarily governed by the column–aspect ratio. This observation is supported by Equation (7), derived from this parameter, which consistently yielded the lowest strength values across multiple specimens, as demonstrated in Appendix A.

Author Contributions: Conceptualization, A.G. and M.H.; methodology, L.A.; software, A.G.; validation, M.H., N.M.A. and L.A.; formal analysis, A.G.; investigation, A.G.; resources, M.H.; data curation, L.A.; writing—original draft preparation, L.A.; writing—review and editing, N.M.A.; visualization, M.H.; supervision, A.G.; project administration, L.A. All authors have read and agreed to the published version of the manuscript.

Funding: This research received no external funding.

Data Availability Statement: All the data generated during the development of this article are included.

Conflicts of Interest: The authors declare no conflict of interest.

Abbreviations

bo & u_p	perimeter for the shear strength calculated at $d/2$ from the column's face
C	depth of the uncracked concrete (mm)
d	slab's depth
E_f	modulus of elasticity of the GFRP bars
E_s	elastic modulus of the steel bars
E_c	elastic modulus of the concrete
f_{pcd} & f'_c	concrete compressive strength (MPa)
k	relation between the neutral axis to the depth of the reinforced GFRP bars
n_f	relation between E_f to E_c
u	column cross-section (mm)
V	shear force (N)
ν_c	shear strength (MPa)
α_s	4.0 for interior slab–column connection
β_c	the relationship between the long to the short side of the column cross-section
β_d	depth's coefficient
β_r	the influence of the loaded area
β_p	effect of the reinforcement ratio
γ_b	safety factor (1.3)
λ	concrete type's coefficient
ϕ_c	material resistance factor
ρ_f	reinforcement ratio

Appendix A

The data in the Tables A1 and A2 were obtained from the literature [22].

Table A1. Available literature.

Slab	L1 (mm)	Supported dim. L1 (mm)	L2 (mm)	Supported dim. L2 (mm)	Column dim. (mm)	Total Depth (mm)	Effective Depth (mm)	f'_c (MPa)	Flexural Reinforcement Type	p_f	E_f (MPa)	*M*/*V*	*Vexp* (kN)
Interior slab–column connections													
[6]													
H-1.0-XX	2800	2600	2800	2600	300	200	160	80	G	0.98	65	0.15	461
H-1.5-XX	2800	2600	2800	2600	300	200	160	84	G	1.46	65	0.15	541
H-2.0-XX	2800	2600	2800	2600	300	200	160	87	G	1.91	65	0.15	604
[5]													
GN-0.65	2800	2600	2800	2600	300	200	160	42	G	0.65	68	0.15	363
GN-0.98	2800	2600	2800	2600	300	200	160	38	G	0.98	68	0.15	378
GN-1.30	2800	2600	2800	2600	300	200	160	39	G	1.30	68	0.15	425
GH-0.65	2800	2600	2800	2600	300	200	160	70	G	0.65	68	0.15	380
[4]													
G-00-XX	2800	2600	2800	2600	300	200	160	38	G	0.65	68	0.00	421
G-30-XX	2800	2600	2800	2600	300	200	160	42	G	0.65	68	0.30	296
R-15-XX	2800	2600	2800	2600	300	200	160	40	G	0.65	63.1	0.15	320
[14]													
G(0.7)30/20	2500	2000	2500	2000	300	200	134	34.3	G	0.71	48.2	0	329
G(1.6)30/20	2500	2000	2500	2000	300	200	131	38.6	G	1.56	48.1	0	431
G(0.7)45/20	2500	2000	2500	2000	450	200	134	44.9	G	0.71	48.2	0	400
G(1.6)45/20	2500	2000	2500	2000	450	200	131	32.4	G	1.56	48.1	0	504
G(0.3)30/35	2500	2000	2500	2000	300	350	284	34.3	G	0.34	48.2	0	825
G(0.7)30/35	2500	2000	2500	2000	300	350	281	39.4	G	0.73	48.1	0	1071
G(0.3)45/35	2500	2000	2500	2000	450	350	284	48.6	G	0.34	48.2	0	911
G(0.7)45/35	2500	2000	2500	2000	450	350	281	29.6	G	0.73	48.1	0	1248
[3]													
G(1.6)30/20-H	2500	2000	2500	2000	300	200	131	75.8	G	1.56	57.4	0	547
G(1.2)30/20	2500	2000	2500	2000	300	200	131	37.5	G	1.21	64.9	0	438
G(1.6)30/35-H	2500	2000	2500	2000	300	350	275	38.2	G	1.61	57.4	0	1492
G(1.6)30/35-H	2500	2000	2500	2000	300	350	275	75.8	G	1.61	57.4	0	1600
[4]													
G(0.7)30/20-B	2500	2000	2500	2000	300	200	134	39	G	0.71	48.2	0	386
G(1.6)30/20-B	2500	2000	2500	2000	300	200	131	32	G	1.56	48.1	0	451
G(1.6)45/20-B	2500	2000	2500	2000	450	200	131	39	G	1.56	48.1	0	511
G(0.3)30/35-B	2500	2000	2500	2000	300	350	284	39	G	0.34	48.2	0	782
G(0.7)30/35-B-1	2500	2000	2500	2000	300	350	281	30	G	0.73	48.1	0	1027
G(0.7)30/35-B-2	2500	2000	2500	2000	300	350	281	47	G	0.73	48.1	0	1195
G(0.3)45/35-B	2500	2000	2500	2000	450	350	284	32	G	0.34	48.2	0	1020
[23]													
GSL-PUNC-0.4	2200	2000	2200	2000	200	150	129	39	G	0.48	48	0	180
GSL-PUNC-0.6	2200	2000	2200	2000	200	150	129	39	G	0.68	48	0	212
GSL-PUNC-0.8	2200	2000	2200	2000	200	150	129	39	G	0.92	48	0	244
[22]													
GFU1	2300	2000	2300	2000	225	150	110	36.3	G	1.18	48.2	0	222
GFB2	2300	2000	2300	2000	225	150	110	36.3	G	2.15	48.2	0	246
GFB3	2300	2000	2300	2000	225	150	110	36.3	G	3	48.2	0	248
[24]													

Table A1. *Cont.*

Slab	L1 (mm)	Supported dim. L1 (mm)	L2 (mm)	Supported dim. L2 (mm)	Column dim. (mm)	Total Depth (mm)	Effective Depth (mm)	f'_c (MPa)	Flexural Reinforcement Type	p_f	E_f (MPa)	*M*/*V*	*Vexp* (kN)
SG1	2000	1700	2000	1700	200	175	142	32	G	0.18	45	0	170
SC1	2000	1700	2000	1700	200	175	142	32.8	G	0.15	110	0	229
SG2	2000	1700	2000	1700	200	175	142	46.4	G	0.38	45	0	271
SG3	2000	1700	2000	1700	200	175	142	30.4	G	0.38	45	0	237
SC2	2000	1700	2000	1700	200	175	142	29.6	G	0.35	110	0	317
					[22]								
GFR-1	2150	1670	2150	1670	250	155	120	29.5	G	0.73	34	0	199
GFR-2	2150	1670	2150	1670	250	155	120	28.9	G	1.46	34	0	249
NEF-1	2150	1670	2150	1670	250	155	120	37.5	G grid	0.87	28.4	0	203
					[25]								
C1	1000	900	1000	900	150 *	120	96	36.7	C grid	0.27	91.8	0	181
C1′	1000	900	1000	900	230 *	120	96	37.3	C grid	0.27	91.8	0	189
C2	1000	900	1000	900	150 *	120	95	35.7	C grid	1.05	95	0	255
C2′	1000	900	1000	900	230 *	120	95	36.3	C grid	1.05	95	0	273
C3	1000	900	1000	900	150 *	150	126	33.8	C grid	0.52	92	0	347
C3′	1000	900	1000	900	230 *	150	126	34.3	C grid	0.52	92	0	343
CS	1000	900	1000	900	150 *	120	95	32.6	C	0.19	147.6	0	142
CS′	1000	900	1000	900	230 *	120	95	33.2	C	0.189	147.6	0	150
H1	1000	900	1000	900	150 *	120	95	118	H grid	0.62	37.3	0	207
H2	1000	900	1000	900	150 *	120	89	35.8	H grid	3.76	40.7	0	231
H2′	1000	900	1000	900	80 *	120	89	35.9	H grid	3.76	40.7	0	171
H3	1000	900	1000	900	150 *	150	122	32.1	H grid	1.22	44.8	0	237
H3′	1000	900	1000	900	80 *	150	122	32.1	H grid	1.22	44.8	0	217
Edge slab–column connections													
					[26]								
G	2500	2000	1350	1150	300	200	160	41.4	G	1.55	53	0.31	314
					[27]								
GSC-1.35	2800	2600	1550	1450	300	200	160	42	G	1.28	60.9	0.40	264
GSC-1.8	2800	2600	1550	1450	300	200	160	42	G	1.7	60.9	0.40	278
					[28]								
H-0.9-XX	2800	2600	1550	1450	300	200	160	81	G	0.85	60.9	0.40	251
H-1.35-XX	2800	2600	1550	1450	300	200	160	85	G	1.28	60.9	0.40	272
H-1.8-XX	2800	2600	1550	1450	300	200	160	80	G	1.7	60.9	0.40	288
					[22]								
RD-XX-M	2800	2600	1550	1450	300	200	160	45.8	G	0.85	60.2	0.40	191
SC-XX-L	2800	2600	1550	1450	300	200	160	49.4	G	0.85	60.9	0.20	239
SC-XX-M	2800	2600	1550	1450	300	200	160	47.3	G	0.85	60.9	0.40	227
SC-XX-H	2800	2600	1550	1450	300	200	160	48.4	G	0.85	60.9	0.60	159

* Circular columns.

Table A2. Available literature (continued).

Slab	$V_{exp,0.5d}$ (MPa)	[7]	[12]	[21]	Proposed Equations			Failure Shear Strength (Vf) ** (MPa)	$V_{exp,0.5d}/Vf$
		$V_{exp,0.5d}/V_{CSA}$	$V_{exp,0.5d}/V_{ACI}$	$V_{exp,0.5d}/V_{JSCE}$	EQ7 (MPa)	EQ8 (MPa)	EQ9 (MPa)		
Interior slab–column connections									
[6]									
H-1.0-XX	2.16	1.14	1.89	1.30	2.24	2.37	2.18	2.18	0.99
H-1.5-XX	2.54	1.18	1.84	1.34	2.60	2.75	2.53	2.53	1.00
H-2.0-XX	2.83	1.20	1.79	1.36	2.89	3.06	2.81	2.81	1.01
[5]									
GN-0.65	1.70	1.15	2.10	1.16	1.60	1.69	1.56	1.56	1.09
GN-0.98	1.77	1.08	1.87	1.05	1.78	1.88	1.73	1.73	1.02
GN-1.30	1.99	1.09	1.84	1.08	1.97	2.08	1.92	1.92	1.04
GH-0.65	1.78	1.07	1.92	1.21	1.90	2.01	1.85	1.85	0.96
[4]									
G-00-XX	1.43	1.00	1.82	0.97	1.55	1.64	1.51	1.51	0.95
G-30-XX	1.77	1.19	2.19	1.21	1.60	1.69	1.56	1.56	1.13
R-15-XX	1.50	1.05	1.94	1.05	1.54	1.62	1.50	1.50	1.00
[14]									
G(0.7)30/20	1.41	1.11	2.08	1.11	1.37	1.39	1.37	1.37	1.03
G(1.6)30/20	1.91	1.11	1.90	1.13	1.86	1.86	1.85	1.85	1.03
G(0.7)45/20	1.28	0.92	1.75	1.04	1.50	1.34	1.53	1.34	0.95
G(1.6)45/20	1.66	1.02	1.73	1.10	1.75	1.56	1.77	1.56	1.06
G(0.3)30/35	1.24	1.25	2.58	1.20	1.08	1.27	1.18	1.08	1.15
G(0.7)30/35	1.64	1.22	2.29	1.20	1.45	1.71	1.60	1.45	1.13
G(0.3)45/35	1.09	0.98	2.07	1.10	1.21	1.33	1.34	1.21	0.90
G(0.7)45/35	1.52	1.24	2.29	1.31	1.32	1.45	1.46	1.32	1.15
[3]									
G(1.6)30/20-H	2.42	1.15	1.85	1.35	2.47	2.48	2.45	2.45	0.99
G(1.2)30/20	1.94	1.12	1.91	1.13	1.87	1.88	1.86	1.86	1.04
G(1.6)30/35-H	2.36	1.28	2.15	1.25	1.98	2.33	2.18	1.98	1.19
G(1.6)30/35-H	2.53	1.18	1.91	1.34	2.49	2.93	2.74	2.49	1.02
[4]									
G(0.7)30/20-B	1.66	1.25	2.35	1.27	1.43	1.45	1.43	1.43	1.16
G(1.6)30/20-B	2.00	1.24	2.10	1.25	1.74	1.75	1.74	1.74	1.15
G(1.6)45/20-B	1.68	0.97	1.67	1.06	1.86	1.65	1.89	1.65	1.02
G(0.3)30/35-B	1.18	1.13	2.36	1.11	1.12	1.32	1.24	1.12	1.05

Table A2. *Cont.*

Slab	$V_{exp,0.5d}$ (MPa)	[7]	[12]	[21]	Proposed Equations			Failure Shear Strength (Vf) ** (MPa)	$V_{exp,0.5d}/Vf$
		$V_{exp,0.5d}/V_{CSA}$	$V_{exp,0.5d}/V_{ACI}$	$V_{exp,0.5d}/V_{JSCE}$	EQ7 (MPa)	EQ8 (MPa)	EQ9 (MPa)		
G(0.7)30/35-B-1	1.57	1.28	2.37	1.26	1.33	1.56	1.46	1.33	1.18
G(0.7)30/35-B-2	1.83	1.28	2.44	1.34	1.54	1.81	1.69	1.54	1.19
G(0.3)45/35-B	1.22	1.26	2.58	1.31	1.05	1.15	1.16	1.05	1.16
				[23]					
GSL-PUNC-0.4	1.06	0.91	1.81	0.87	1.26	1.39	1.23	1.23	0.86
GSL-PUNC-0.6	1.25	0.96	1.81	0.92	1.41	1.56	1.38	1.38	0.90
GSL-PUNC-0.8	1.44	0.99	1.81	0.95	1.56	1.72	1.53	1.53	0.94
				[22]					
GFU1	1.51	0.98	1.73	0.96	1.66	1.72	1.57	1.57	0.96
GFB2	1.67	0.89	1.47	0.87	2.03	2.10	1.92	1.92	0.87
GFB3	1.68	0.80	1.28	0.78	2.26	2.34	2.14	2.14	0.78
				[24]					
SG1	0.88	1.14	2.58	1.06	0.83	0.93	0.86	0.83	1.06
SC1	1.18	1.20	2.46	1.11	1.06	1.19	1.09	1.06	1.11
SG2	1.40	1.25	2.62	1.24	1.21	1.36	1.24	1.21	1.16
SG3	1.22	1.26	2.56	1.18	1.05	1.18	1.08	1.05	1.16
SC2	1.63	1.29	2.36	1.22	1.36	1.53	1.40	1.36	1.20
				[22]					
GFR-1	1.12	1.03	1.99	1.04	1.17	1.21	1.19	1.17	0.96
GFR-2	1.40	1.03	1.82	1.04	1.47	1.51	1.49	1.47	0.95
NEF-1	1.14	0.97	1.91	0.96	1.27	1.31	1.28	1.27	0.90
				[25]					
C1	2.05	1.76	3.44	1.61	1.26	1.50	1.35	1.26	1.63
C1′	1.64	1.39	2.73	1.38	1.27	1.38	1.38	1.27	1.29
C2	2.94	1.59	2.64	1.46	1.99	2.36	2.13	1.99	1.48
C2′	2.40	1.29	2.15	1.28	2.00	2.17	2.17	2.00	1.20
C3	2.65	1.87	3.36	1.65	1.53	1.89	1.68	1.53	1.73
C3′	2.06	1.45	2.59	1.37	1.54	1.77	1.71	1.54	1.34
CS	1.64	1.40	2.67	1.30	1.26	1.50	1.35	1.26	1.30
CS′	1.32	1.12	2.14	1.11	1.27	1.38	1.38	1.27	1.04
H1	2.38	1.77	3.03	1.92	1.82	2.16	1.95	1.82	1.31
H2	2.92	1.37	2.18	1.27	2.30	2.69	2.44	2.30	1.27
H2′	3.00	1.41	2.24	1.17	2.30	2.94	2.42	2.30	1.31

Table A2. *Cont.*

Slab	$V_{exp,0.5d}$ (MPa)	[7]	[12]	[21]	Proposed Equations			Failure Shear Strength (Vf) ** (MPa)	$V_{exp,0.5d}/Vf$
		$V_{exp,0.5d}/V_{CSA}$	$V_{exp,0.5d}/V_{ACI}$	$V_{exp,0.5d}/V_{JSCE}$	EQ7 (MPa)	EQ8 (MPa)	EQ9 (MPa)		
H3	1.90	1.31	2.30	1.17	1.57	1.93	1.73	1.57	1.21
H3′	2.30	1.58	2.78	1.28	1.57	2.06	1.71	1.57	1.46
Mean	-	1.20	2.18	1.19	-	-	-	-	1.11
SD	-	0.22	0.43	0.20	-	-	-	-	0.18
COV (%)	-	18.3	19.7	16.6	-	-	-	-	16.4
Edge slab–column connections									
				[26]					
G	2.43	1.26	2.16	1.23	1.96	2.32	2.02	1.96	1.24
				[27]					
GSC-1.35	2.36	1.32	2.26	1.27	1.93	2.29	1.88	1.88	1.25
GSC-1.8	2.48	1.26	2.10	1.21	2.13	2.52	2.07	2.07	1.20
				[28]					
H-0.9-XX	2.24	1.27	2.16	1.38	2.10	2.49	2.04	2.04	1.10
H-1.35-XX	2.43	1.21	1.92	1.31	2.45	2.90	2.38	2.38	1.02
H-1.8-XX	2.57	1.16	1.82	1.26	2.64	3.12	2.57	2.57	1.00
				[22]					
RD-XX-M	1.71	1.10	1.99	1.05	1.73	2.05	1.68	1.68	1.02
SC-XX-L	1.50	1.00	1.79	0.93	1.78	2.11	1.73	1.73	0.87
SC-XX-M	2.03	1.32	2.37	1.25	1.76	2.08	1.71	1.71	1.19
SC-XX-H	1.84	1.23	2.19	1.13	1.77	2.09	1.72	1.72	1.07
Mean	-	1.22	2.08	1.20	-	-	-	-	1.10
SD	-	0.10	0.18	0.12	-	-	-	-	0.12
COV (%)	-	8.27	8.71	10.4	-	-	-	-	10.7

** The failure shear strength (Vf) is the least value obtained from the proposed Equations (7)–(9).

References

1. Aslam, F.; AbdelMongy, M.; Alzara, M.; Ibrahim, T.; Deifalla, A.F.; Yosri, A.M. Two-Way Shear Resistance of FRP Reinforced-Concrete Slabs: Data and a Comparative Study. *Polymers* **2022**, *14*, 3799. [CrossRef] [PubMed]
2. Shi, J.; Sun, S.; Cao, X.; Wang, H. Pullout Behaviors of Basalt Fiber-Reinforced Polymer Bars with Mechanical Anchorages for Concrete Structures Exposed to Seawater. *Constr. Build. Mater.* **2023**, *373*, 130866. [CrossRef]
3. Hassan, M.; Ahmed, E.; Benmokrane, B. Punching Shear Strength of Glass Fiber-Reinforced Polymer Reinforced Concrete Flat Slabs. *Can. J. Civ. Eng.* **2013**, *40*, 951–960. [CrossRef]
4. Hassan, M.; Ahmed, E.; Benmokrane, B. Punching-Shear Strength of Normal and High-Strength Two-Way Concrete Slabs Reinforced with GFRP Bars. *ASCE J. Compos. Constr.* **2013**, *17*, 04013003. [CrossRef]
5. Gouda, A.; El-Salakawy, E.F. Punching Shear Strength of GFRP-RC Interior Slab–Column Connections Subjected to Moment Transfer. *ASCE J. Compos. Constr.* **2015**, *20*, 04015037. [CrossRef]
6. Hussein, A.; El-Salakawy, E.F. Punching Shear Behavior of Glass Fiber-Reinforced Polymer-Reinforced Concrete Slab-Column Interior Connections. *ACI Struct. J.* **2018**, *115*, 1075–1088. [CrossRef]
7. *CAN/CSAS806-12*; Design and Construction of Building Components with Fiber Reinforced Polymers. Canadian Standards Association (CSA): Toronto, ON, Canada, 2012.
8. Cervenka, V.; Jendele, L.; Cervenka, J. *ATENA Program Documentation Part 1: Theory*; Cervenka Consulting Ltd.: Prague, Czech Republic, 2013.
9. CEB-FIB. *Model Code for Concrete Structures*; Comite Euro-International Du Beton, Thomas Telford Ltd.: London, UK, 1990.
10. Hordijk, D.A. Local Approach to Fatigue of Concrete. PhD Thesis, Delft University of Technology, Delft, The Netherlands, 1991. ISBN 90/9004519-8.
11. Alves, J.; El-Ragaby, A.; El-Salakawy, E. Durability of GFRP Bars' Bond to Concrete under Different Loading and Environmental Conditions. *ASCE J. Compos. Constr.* **2011**, *15*, 249–262. [CrossRef]
12. American Concrete Institute (ACI) Committee 440. *Guide for the Design and Construction of Structural Concrete Reinforced with Fiber-Reinforced Polymer Bars. ACI 440.1R-22*; American Concrete Institute (ACI): Farmington Hills, MI, USA, 2022; 83p.
13. Hawkins, N.M.; Fallsen, H.B.; Hinojosa, R.C. Influence of Column Rectangularity on the Behaviour of Flat Plate Structures; in Cracking, Deflection and Ultimate Load of Concrete Slab System. *ACI Spec. Publ.* **1971**, *30*, 127–146.
14. Dulude, C.; Hassan, M.; Ahmed, E.; Benmokrane, B. Punching Shear Behavior of Flat Slabs Reinforced with Glass Fiber-Reinforced Polymer Bars. *ACI Struct. J.* **2013**, *110*, 723–734.
15. Sherif, A.G.; Emara, M.B.; Ibrahim, A.H.; Magd, S.A. Effect of the Column Dimensions on the Punching Shear Strength of Edge Column-Slab Connections. *ACI Struct. J.* **2005**, *232*, 175–192.
16. Marzouk, H.; Hussein, A. Experimental Investigation on the Behaviour of High-Strength Concrete Slabs. *ACI Struct. J.* **1991**, *88*, 701–713.
17. Lovrovich, J.S.; McLean, D.A. Punching Shear Behaviour of Slabs with Varying Span-Depth Ratios. *ACI Struct. J.* **1990**, *87*, 507–512.
18. American Concrete Institute (ACI) Committee 318. *Building Code Requirments for Structural Concrete. ACI 318-83 and Commentary*; American Concrete Institute (ACI): Detroit, MI, USA, 1983; 111p.
19. Ospina, C.E. Alternative Model for Concentric Punching Capacity Evaluation of Reinforced Concrete Two-Way Slabs. *Concr. Int.* **2005**, *27*, 53–57.
20. American Concrete Institute (ACI) Committee 440. *Guide for the Design and Construction of Structural Concrete Reinforced with FRP Bars. ACI 440.1R-06*; American Concrete Institute (ACI): Farmington Hills, MI, USA, 2006; 44p.
21. Japan Society of Civil Engineers (JSCE). *Recommendation for Design and Construction of Concrete Structures Using Continuous Fiber Reinforcing Materials*; Japan Society of Civil Engineers (JSCE): Tokyo, Japan, 1997.
22. El-Gendy, M.G.; El-Salakawy, E.F. Assessment of Punching Shear Design Models for FRP-RC Slab–Column Connections. *ASCE J. Compos. Constr.* **2020**, *24*, 04020047. [CrossRef]
23. Nguyen-Minh, L.; Rovňák, M. Punching Shear Resistance of Interior GFRP Reinforced Slab-Column Connections. *ASCE J. Compos. Constr.* **2013**, *17*, 2–13. [CrossRef]
24. El-Ghandour, A.W.; Pilakoutas, K.; Waldron, P. Punching Shear Behavior of Fiber Reinforced Polymers Reinforced Concrete Flat Slabs: Experimental Study. *ASCE J. Compos. Constr.* **2003**, *7*, 258–265. [CrossRef]
25. Matthys, S.; Taerwe, L. Concrete Slabs Reinforced with FRP Grids. II: Punching Resistance. *ASCE J. Compos. Constr.* **2000**, *4*, 154–161. [CrossRef]
26. Salama, A.E.; Hassan, M.; Benmokrane, B. Effectiveness of Glass Fiber-Reinforced Polymer Stirrups as Shear Reinforcement in Glass Fiber-Reinforced Polymer- Reinforced Concrete Edge Slab-Column Connections. *ACI Struct. J.* **2019**, *116*, 97–112. [CrossRef]
27. El-Gendy, M.G.; El-Salakawy, E.F. Effect of Shear Studs and High Moments on Punching Behavior of GFRP-RC Slab–Column Edge Connections. *ASCE J. Compos. Constr.* **2016**, *20*, 04016007. [CrossRef]
28. Mostafa, A.M.; El-Salakawy, E.F. Behavior of GFRP-RC Slab–Column Edge Connections with High-Strength Concrete and Shear Reinforcement. *ASCE J. Compos. Constr.* **2018**, *22*, 04018001. [CrossRef]